Vibration Control of a Cantilever Beam with Time Delay State Feedback

Atef F. El-Bassiouny

Department of Mathematics, Faculty of Science, Benha University, Benha 13518, Egypt

Reprint requests to A. F. E.-B.; E-mail: elbassiouny_af@yahoo.com

Z. Naturforsch. **61a,** 629 – 640 (2006); received June 6, 2006

The primary and subharmonic resonance of order one-third of a cantilever beam under state feedback control with a time delay are investigated. Using the method of multiple scales, we obtain two slow flow equations for the amplitude and phase. The first-order approximate solution is derived and the effect of time delay on the resonance is investigated. The concept of an equivalent damping, related to the delay feedback, is proposed and an appropriate choice of the feedback gains and the time delay is discussed from the viewpoint of vibration control. The fixed points corresponding to the periodic motion of the starting system are determined, and the frequency-response and external excitation-response curves are shown. Bifurcation analysis is conducted in order to examine the stability of the system.

Key words: Cantilever Beam; Time Delay; Vibration Control; Resonance; Periodic Motion; Saddle Node Bifurcation.

1. Introduction

In the last years, many papers have been devoted to the control of resonantly forced systems in various engineering fields. In passive vibration absorbers a physical device is connected with the primary structure, while in the case of active absorbers the device is replaced by a control system of sensors, actuators and filters. Active control of mechanical and structural vibrations is superior to passive control, because the former is more flexible in many aspects.

Periodically forced nonlinear systems under delay control have been analyzed by Plaut and Hsieh [1] in the case of nonlinear structural vibrations with a time delay in damping. Palkovics and Venhovens [2] investigated the stability and possible chaotic motions in the controlled wheel suspension system. Belair and Cambell [3] analyzed the stability and bifurcation of equilibria in a multi-delayed differential equation. Diekmann et al. [4] performed a nonlinear analysis for determining Hopf bifurcations in systems of autonomous differential equations. Stepan and Haller [5] considered quasi-periodic oscillations in robot dynamics, and Moiola et al. [6] dealt for a more general forced nonlinear system under delay control the response amplitude in the parametric excitation-response curve, while the velocity feedback stabilizes the trivial solution in the frequency-response curve. Thomsen [7] investigated the vibration suppression by using self-arranging mass effects of adding restoring force. Yabuno [8] proposed a control law based on linear velocity feedback and linear and cubic velocity feedback. His studies demonstrated that nonlinear position feedback reduces the response amplitude in the parametric excitation-response curve, while linear velocity feedback stabilizes the trivial solution in the frequency-response curve. Hu et al. [9] investigated the resonances of a harmonically forced Duffing oscillator with time delay feedback. Using the method of multiple scales, they demonstrated that appropriate choices of feedback gain and the time delay are possible for a better vibration control. Hy and Zh [10] considered controlled mechanical systems with time delays, and in particular primary resonance and subharmonic resonance of a harmonically forced Duffing oscillator with time delay. The stability of periodic motion and applications to active chassis of ground vehicles are discussed. Maccari [11] studied the parametric resonance of a van der Pol oscillator under state feedback control with time delay. Faria [12] investigated stability and bifurcation of a delayed predator-prey model and effect of diffusion. Liao and Chen [13] studied the local stability, Hopf and resonant codimension-two bifurcation in a harmonic oscillator with two time delays. Meng and Wei [14] analyzed the stability and bifurcation of a mutual system with time delay. Yuan and Han [15] analyzed the bifurcation of a chemostat model with two distributed delays. Fofance and Ryba [16] investigated

the parametric stability of nonlinear time delay equations. Leung et al. [17] investigated the resonance control for a forced single-degree-of-freedom nonlinear system. Sun et al. [18] analyzed the chaotic behavior of a double-well Duffing oscillator with both delayed displacement and velocity feedbacks under a harmonic excitation. Li et al. [19] studied the nonlinear dynamics of a Duffing-van der Pol oscillator under linear-plus-nonlinear state feedback control with time delay. El-Bassiouny [20] investigated fundamental and subharmonic resonances of harmonical oscillation with delay state feedback. Kouda and Mori [21] analyzed a ring of mutually coupled van der Pol oscillators with coupling delay. Oueni et al. [22] have considered a nonlinear active vibration absorber coupled with the plant through user-defined cubic nonlinearities. If the plant is excited at primary resonance and the absorber frequency is equal to the plant natural frequency, they demonstrated that when the forcing amplitude increases beyond a certain threshold, high-amplitude vibrations are suppressed because the response amplitude of the plant remains constant, while the response amplitude of the absorber increases. Oueni et al. [23] studied the saturation phenomenon in devising an active vibration suppression technique. A plant was coupled with a second-order absorber through a user-defined quadratic feedback control law. They demonstrated that, by tuning the natural frequency of the absorber to one-half the excitation frequency, effective vibration suppression is possible. El-Bassiouny [24] studied an approach for implementing an active nonlinear vibration absorber. The strategy exploits the saturation phenomenon that is exhibited by multi-degree-of-freedom systems with cubic nonlinearities possessing one-to-one internal resonance. The proposed technique consists of introducing a second-order controller and coupling it to the plant through a sensor and an actuator, where both the feedback and control signals are cubic. El-Bassiouny [25] studied the vibration and chaos control of nonlinear torsional vibrating systems.

In this paper a cantilever beam, whose response is governed by a nonlinear partial differential equation, is considered. If we focus on a mode that is not involved in an internal resonance with any of the other modes, then application of a single-mode discretization scheme (see [26]) yields the nonlinear differential equation

$$\frac{\mathrm{d}^2X(t)}{\mathrm{d}t^2}+\mu\frac{\mathrm{d}X(t)}{\mathrm{d}t}+X(t)+\alpha X^3(t)+\beta\dot{X}(t)X^2(t)+\gamma\ddot{X}(t)X^2(t)=uX(t-\tau)+v\frac{\mathrm{d}X(t-\tau)}{\mathrm{d}t}+H\cos\Phi t, \tag{1}$$

where a dot denotes differentiation with respect to time, μ is a damping factor, α the curvature nonlinearity coefficient, β and γ are the inertia nonlinearity coefficients, H is the forcing amplitude and Φ the external excitation frequency. u and v are the feedback gains and τ is the time delay.

In the following two sections, the primary and the one-third subharmonic resonances will be studied by using the multiple scale perturbation technique. Presented in Section 4 are the numerical results of the above two cases and their discussion. Section 5 presents the concluding remarks for the frequency-response and external excitation-response curves of the two cases.

2. Primary Resonance

To investigate the primary resonance of the delay-controlled system (1) by using the multiple scale perturbation technique [27–31], we confine the study to small damping, weak nonlinearities, weak feedback and soft excitation. That is

$$\begin{aligned}&\mu=O(\varepsilon),\quad \alpha=O(\varepsilon),\quad \beta=O(\varepsilon),\\ &\gamma=O(\varepsilon),\quad u=O(\varepsilon),\quad v=O(\varepsilon),\\ &H=O(\varepsilon),\quad \Phi-1=\varepsilon\sigma,\quad \sigma=O(\varepsilon),\end{aligned} \tag{2}$$

where $0<\varepsilon\ll 1$ and σ is the detuning parameter. We rewrite (1) as

$$\frac{\mathrm{d}^2X(t)}{\mathrm{d}t^2}+X(t)=-\mu\frac{\mathrm{d}X(t)}{\mathrm{d}t}-\alpha X^3(t)-\beta\dot{X}(t)X^2(t)-\gamma\ddot{X}(t)X^2(t)+uX(t-\tau)+v\frac{\mathrm{d}X(t-\tau)}{\mathrm{d}t}+H\cos(1+\varepsilon\sigma t). \tag{3}$$

For simplicity we assume a two scale expansion of the form

$$\begin{aligned}&X(t)=X_0(T_0,T_1)+X_1(T_0,T_1)+O(\varepsilon^2),\\ &T_r=\varepsilon^r t,\quad r=0,1\end{aligned} \tag{4}$$

and use the following differential operators:

$$\begin{aligned}&\frac{\mathrm{d}}{\mathrm{d}t}=\frac{\partial}{\partial T_0}.+\varepsilon\frac{\partial}{\partial T_1}.+O(\varepsilon^2)=D_0+\varepsilon D_1+O(\varepsilon^2),\\ &\frac{\mathrm{d}^2}{\mathrm{d}t^2}=D_0^2+2\varepsilon D_0D_1+O(\varepsilon^2).\end{aligned} \tag{5}$$

Substituting (4) and (5) into (3) and equating the coefficients of the same power of ε, we obtain a set of linear partial differential equations:

$$D_0^2 X_0(T_0,T_1) + X_0(T_0,T_1) = 0, \tag{6}$$

$$\begin{aligned} &D_0^2 X_1(T_0,T_1) + X_1(T_0,T_1) = \\ &-2D_0D_1X_0(T_0,T_1) - 2\mu D_0X_0(T_0,T_1) \\ &-\alpha X_0^3(T_0,T_1) - \beta X_0(T_0,T_1)(D_0X_0(T_0,T_1))^2 \\ &-\gamma X_0^2(T_0,T_1)D_0^2X_0(T_0,T_1) + 2uX_0(T_0-\tau,T_1) \\ &+2vD_0X_0(T_0-\tau,T_1) + H\cos(1+\varepsilon\sigma t). \end{aligned} \tag{7}$$

Solving (6) for $X_0(T_0,T_1)$, we have

$$X_0(T_0,T_1) = R(T_1)\exp(\mathrm{i}T_0) + \mathrm{cc}, \tag{8}$$

where cc denotes the complex conjugate of the preceding terms and

$$R(T_1) = \frac{1}{2}\rho(T_1)\exp\{\mathrm{i}\theta(T_1)\}. \tag{9}$$

Substituting (8) into (7), we obtain

$$\begin{aligned} &D_0^2 X_1(T_0,T_1) + X_1(T_0,T_1) = \\ &-2\mathrm{i}(D_1R+\mu R)\exp(\mathrm{i}T_0) - \alpha(R^3\exp(3\mathrm{i}T_0) \\ &+3R^2\overline{R}\exp(\mathrm{i}T_0)) - \beta R^2\overline{R}\exp(\mathrm{i}T_0) \\ &+3\gamma R^2\overline{R}\exp(\mathrm{i}T_0) + 2uR\exp(\mathrm{i}T_0)\exp(-\mathrm{i}\tau) \\ &+2\mathrm{i}vR\exp(\mathrm{i}T_0)\exp(-\mathrm{i}\tau) \\ &+\frac{1}{2}H\exp(\mathrm{i}T_0)\exp(\mathrm{i}\sigma T_0) + \mathrm{cc}, \end{aligned} \tag{10}$$

where $\overline{R}$ is the complex conjugate of R. To eliminate the secular term in (10), we let

$$\begin{aligned} &-2\mathrm{i}(D_1R+\mu R) - 3\alpha R^2\overline{R} - \beta R^2\overline{R} + 3\gamma R^2\overline{R} \\ &+2uR\exp(-\mathrm{i}\tau) + 2\mathrm{i}vR\exp(-\mathrm{i}\tau) \\ &+\frac{1}{2}H\exp(\mathrm{i}\sigma T_0) = 0. \end{aligned} \tag{11}$$

By substituting (9) into (11) and separating the real and imaginary parts, we obtain a set of autonomous differential equations that govern the amplitude $\rho(T_1)$ and the phase $\phi(T_1)$:

$$D_1\rho = -\mu\rho - u\rho\sin\tau + v\rho\cos\tau - \frac{1}{2}H\sin\phi, \tag{12}$$

$$\begin{aligned} \rho D_1\phi = \sigma\rho - \frac{3}{8}(\alpha+\beta-\gamma)\rho^3 + u\rho\cos\tau \\ + v\rho\sin\tau + \frac{1}{2}H\cos\phi, \end{aligned} \tag{13}$$

where

$$\phi(T_1) = \sigma T_1 - \theta(T_1). \tag{14}$$

From (12) and (13) we get a set of algebraic equations for the amplitude ρ and phase ϕ of the steady-state fundamental resonance:

$$-\mu\rho - u\rho\sin\tau + v\rho\cos\tau - \frac{1}{2}H\sin\phi = 0, \tag{15}$$

$$\begin{aligned} &\sigma\rho - \frac{3}{8}(\alpha+\beta-\gamma)\rho^3 + u\rho\cos\tau + v\rho\sin\tau \\ &+\frac{1}{2}H\cos\phi = 0, \end{aligned} \tag{16}$$

whereby we derive the frequency-response relation between ρ and σ, and that between ϕ and σ:

$$\begin{aligned} &(\mu + u\sin\tau - v\cos\tau)^2\rho^2 \\ &+\left(\sigma + \zeta\cos\tau + \eta\sin\tau - \frac{3}{8}(\alpha+\beta-\gamma)\rho^2\right)\rho^2 \\ &-\frac{1}{4}H^2 = 0, \end{aligned} \tag{17}$$

$$\tan\phi + \frac{\mu + u\sin\tau - v\cos\tau}{\sigma + u\cos\tau + v\sin\tau - \frac{3}{8}(\alpha+\beta-\gamma)\rho^2} = 0. \tag{18}$$

The first approximation for the fundamental resonance reads

$$X(t) = \rho\cos(\Phi t - \phi) + O(\varepsilon). \tag{19}$$

To determine the stability of the steady-state motions, one lets

$$\rho = \rho_0 + \rho_1, \quad \phi = \phi_0 + \phi_1, \tag{20}$$

where ρ_0 and ϕ_0 are solutions of (15) and (16). Substituting (20) into (12) and (13), using (15) and (16), and keeping only the linear terms in ρ_1 and ϕ_1, one obtains

$$\rho_1' = -(\mu + u\sin\tau - v\cos\tau)\rho_1 + \frac{1}{2}(H\cos\phi_0)\phi_1, \tag{21}$$

$$\begin{aligned} \phi_1' = &\left(\frac{\sigma}{\rho_0} - \frac{9\rho_0}{8}(\alpha+\beta-\gamma) + \frac{u}{\rho_0}\cos\tau + \frac{v}{\rho_0}\sin\tau\right) \\ &\cdot\rho_1 - \frac{1}{2\rho_0}(H\sin\phi_0)\phi_1. \end{aligned} \tag{22}$$

Equations (21) and (22) admit solutions of the form

$$(\rho_1,\phi_1) = (d_1,d_2)\exp(\lambda T_1), \tag{23}$$

where d_1 and d_2 are arbitrary constants and

$$\begin{aligned}&\lambda^2+\left\{(\mu+u\sin\tau-v\cos\tau)+\frac{H}{2\rho_0}\sin\phi_0\right\}\lambda\\&+\frac{H}{2\rho_0}(\mu+u\sin\tau-v\cos\tau)\sin\phi_0\\&-\frac{H}{2}\Big(\frac{\sigma}{\rho_0}-\frac{9\rho_0}{8}(\alpha+\beta-\gamma)+\frac{u}{\rho_0}\cos\tau+\frac{v}{\rho_0}\sin\tau\Big)\\&\quad\cdot\cos\phi_0=0.\end{aligned}\tag{24}$$

From the Routh-Hurwitz criterion the steady-state solution is asymptotically stable if and only if the following inequalities hold simultaneously:

$$\left\{(\mu+u\sin\tau-v\cos\tau)+\frac{H}{2\rho_0}\sin\phi_0\right\}>0,\tag{25}$$

$$\begin{aligned}&\left\{(\mu+u\sin\tau-v\cos\tau)\tan\phi_0-\sigma\right.\\&\quad\left.+\frac{9\rho_0^2}{8}(\alpha+\beta-\gamma)-u\cos\tau-v\sin\tau\right\}>0.\end{aligned}\tag{26}$$

Thus, the stable and unstable solutions may be represented by solid and dotted lines on the response curves, respectively.

3. Subharmonic Resonance of Order One-Third

To study the subharmonic resonance of order one-third of the controlled system, we confine ourselves to the case of

$$\begin{aligned}&\mu=O(\varepsilon),\quad \alpha=O(\varepsilon),\quad \beta=O(\varepsilon),\\&\gamma=O(\varepsilon),\quad u=O(\varepsilon),\quad v=O(\varepsilon),\\&H=O(1),\quad \Phi-3=\varepsilon\sigma,\quad \sigma=O(1),\end{aligned}\tag{27}$$

but omit excitations of the small magnitude. Rewrite (1) as

$$\begin{aligned}&\frac{\mathrm{d}^2X(t)}{\mathrm{d}t^2}+X(t)=-\mu\frac{\mathrm{d}X(t)}{\mathrm{d}t}-\alpha X^3(t)\\&-\beta\dot{X}(t)X^2(t)-\gamma\ddot{X}(t)X^2(t)+uX(t-\tau)\\&+v\frac{\mathrm{d}X(t-\tau)}{\mathrm{d}t}+H\cos(3+\varepsilon\sigma t).\end{aligned}\tag{28}$$

Substituting (4) and (5) into (28) and equating the coefficients of the same power of ε, we obtain a set of linear partial differential equations:

$$D_0^2X_0(T_0,T_1)+X_0(T_0,T_1)=H\cos(3T_0+\sigma T_1),\tag{29}$$

$$\begin{aligned}&D_0^2X_1(T_0,T_1)+X_1(T_0,T_1)=\\&-2D_0D_1X_0(T_0,T_1)-2\mu D_0X_0(T_0,T_1)\\&-\alpha X_0^3(T_0,T_1)-\beta X_0(T_0,T_1)\,(D_0X_0(T_0,T_1))^2\\&-\gamma X_0^2(T_0,T_1)D_0^2X_0(T_0,T_1)\\&+2uX_0(T_0-\tau,T_1)+2vD_0X_0(T_0-\tau,T_1).\end{aligned}\tag{30}$$

Solving (29) for $X_0(T_0,T_1)$, we have

$$\begin{aligned}&X_0(T_0,T_1)=\\&R(T_1)\exp(\mathrm{i}T_0)+G\exp\{\mathrm{i}(3T_0+\sigma T_1)\}+\mathrm{cc},\\&G=\frac{H}{2(1-\Phi^2)}.\end{aligned}\tag{31}$$

Substituting (31) into (30), we get

$$\begin{aligned}&D_0^2X_1(T_0,T_1)+X_1(T_0,T_1)=\\&-2\mathrm{i}(D_1R+\mu R)\exp(iT_0)\\&-\alpha\left(3R^2\overline{R}+6RG\overline{G}+3\overline{R}^2G\exp(\mathrm{i}\sigma T_0)\right)\exp(\mathrm{i}T_0)\\&-\beta\left(R^2\overline{R}+18RG\overline{G}-5\overline{R}^2G\exp(\mathrm{i}\sigma T_0)\right)\exp(\mathrm{i}T_0)\\&+\gamma\left(3R^2\overline{R}+38AG\overline{G}+11\overline{R}^2G\exp(\mathrm{i}\sigma T_0)\right)\exp(\mathrm{i}T_0)\\&+2\mathrm{i}uR\exp(\mathrm{i}\sigma T_0)\exp(-\mathrm{i}\tau)\\&+2\mathrm{i}vR\exp(\mathrm{i}T_0)\exp(-\mathrm{i}\tau)+\mathrm{NST}+\mathrm{cc},\end{aligned}\tag{32}$$

where NST stands for the terms that do not produce secular terms. The secular term of (32) vanishes if and only if

$$\begin{aligned}&-2\mathrm{i}(D_1R+\mu R)-(3\alpha+5\beta-3\gamma)R^2\overline{R}\\&-(6\alpha+18\beta-38\gamma)RG\overline{G}\\&-(3\alpha+5\beta-11\gamma)\overline{R}^2G\exp(\mathrm{i}\sigma T_0)\\&+2\mathrm{i}uR\exp(-\mathrm{i}\tau)+2\mathrm{i}vR\exp(-\mathrm{i}\tau)=0.\end{aligned}\tag{33}$$

Substituting (9) into (33) and separating the real and imaginary parts, we obtain the autonomous differential equations that govern the amplitude $\rho(T_1)$ and the phase $\phi(T_1)$:

$$\begin{aligned}D_1\rho=&-\mu\rho-\frac{1}{4}(3\alpha-5\beta-11\gamma)\rho^2G\sin\phi\\&-u\rho\sin\tau+v\rho\cos\tau,\end{aligned}\tag{34}$$

$$\begin{aligned}\rho(D_1\phi-\sigma)=&-\frac{3}{8}(3\alpha+\beta-3\gamma)\rho^3\\&-3(3\alpha+9\beta-19\gamma)\rho G^2\\&-\frac{3}{4}(3\alpha+\beta-11\gamma)\rho^2G\cos\phi\\&+3u\rho\cos\tau+3v\rho\sin\tau,\end{aligned}\tag{35}$$

where

$$\phi(T_1) = \sigma T_1 - 3\theta(T_1). \tag{36}$$

From (34) and (35), we get a set of algebraic equations for the amplitude ρ and phase ϕ of the steady-state principal resonance of order one-half:

$$\begin{aligned} &-\mu\rho - \frac{1}{4}(3\alpha - 5\beta - 11\gamma)\rho^2 G\sin\phi \\ &- u\rho\sin\tau + v\rho\cos\tau = 0, \end{aligned} \tag{37}$$

$$\begin{aligned} &\frac{1}{3}\sigma\rho - \frac{1}{8}(3\alpha + \beta - 3\gamma)\rho^3 - (3\alpha + 9\beta - 19\gamma)\rho G^2 \\ &- \frac{1}{4}(3\alpha - 5\beta - 11\gamma)\rho^2 G\cos\phi + u\rho\cos\tau \\ &+ v\rho\sin\tau = 0. \end{aligned} \tag{38}$$

Equations (37) and (38) show that there are two possibilities: $\rho = 0$ (trivial solution) or $\rho \neq 0$ (non-trivial solution). When $\rho \neq 0$, we have

$$\mu + u\sin\tau - v\cos\tau = -\frac{1}{4}(3\alpha - 5\beta - 11\gamma)\rho G\sin\phi, \tag{39}$$

$$\begin{aligned} &\frac{1}{3}\sigma - \frac{1}{8}(3\alpha + \beta - 3\gamma)\rho^2 - (3\alpha + 9\beta - 19\gamma)G^2 \\ &+ u\cos\tau + v\sin\tau = \frac{1}{4}(3\alpha - 5\beta - 11\gamma)\rho G\cos\phi, \end{aligned} \tag{40}$$

whereby we derive the frequency-response relation between ρ and σ, and that between ϕ and σ:

$$\begin{aligned} &(\mu + u\sin\tau - v\cos\tau)^2 + \left(\frac{1}{3}\sigma - \frac{1}{8}(3\alpha + \beta - 3\gamma)\rho^2\right. \\ &\left. - (3\alpha + 9\beta - 19\gamma)G^2 + u\cos\tau + v\sin\tau\right)^2 \\ &- \frac{1}{16}(3\alpha - 5\beta - 11\gamma)^2\rho^2 G^2 = 0, \end{aligned} \tag{41}$$

$$\begin{aligned} &\tan\phi + \left[u + v\sin\tau - v\cos\tau\right] \\ &\cdot \left[\frac{1}{3}\sigma - \frac{1}{8}(3\alpha + \beta - 3\gamma)\rho^2 - (3\alpha + 9\beta - 19\gamma)G^2\right. \\ &\left. + u\cos\tau + v\sin\tau\right]^{-1} = 0. \end{aligned} \tag{42}$$

Then, the first-order approximation for the steady-state principal harmonic resonance of order one-third is given by

$$X(t) = \rho\cos\left(\frac{\Phi t - \phi}{3}\right) + \frac{H}{1 - \Phi^2}\cos(\Phi t) + O(\varepsilon). \tag{43}$$

The stability of the steady-state subharmonic resonance is determined by substituting (20) into (34) and (35) and linearizing the resulting equations to obtain

$$\begin{aligned} \rho_1' = &-(\mu + u\sin\tau - v\cos\tau)\rho_1 \\ &- \frac{1}{4}\left((3\alpha - 5\beta - 11\gamma)G\rho_0^2\cos\phi_0\right)\phi_1, \end{aligned} \tag{44}$$

$$\begin{aligned} \phi_1' = &\left(\frac{\sigma}{\rho_0} + \frac{u}{\rho_0}\cos\tau + \frac{v}{\rho_0}\sin\tau - \frac{9\rho_0}{8}(3\alpha + \beta - 3\gamma)\right. \\ &- \frac{3}{\rho_0}(3\alpha + 9\beta - 19\gamma)G^2 \\ &\left. - \frac{1}{2}\left((3\alpha - 5\beta - 11\gamma)\rho_0\cos\phi_0\right)\right)\rho_1 \\ &+ \frac{1}{4}\left((3\alpha - 5\beta - 11\gamma)\rho_0\sin\phi_0\right)\phi_1. \end{aligned} \tag{45}$$

Inserting (23) into (44) and (45), the solution is stable if and only if the real part of each of the eigenvalues of the coefficients of the obtained matrix is smaller than zero.

4. Numerical Results and Discussion

The results are presented graphically by using a numerical method. The frequency equations (21) and (41) are nonlinear equations of the amplitude ρ. The numerical results are plotted in Figs. 1–23, which in Figs. 1–6 show the dependence of the response amplitude ρ on the detuning parameter σ for (21), and in Figs. 13–18 for (41) and represent the dependence of the amplitude ρ on the coefficient of external excitation H in Figs. 7–12 for (21) and in Figs. 19–23 for (41).

The stability of a fixed-point solution is studied by examining of the eigenvalues of the Jacobian matrix of (14) and (15) for primary resonance and of (44) and (45) for subharmonic resonance, evaluated at the fixed point of interest. If all eigenvalues have negative real parts, the fixed point is expected to settle on it. These solutions are called stable modes and are given by solid lines in the frequency-response curves of Figs. 1–23. If a pure real eigenvalue becomes positive, the fixed point loses its stability and the motion is expected to diverge from it. These unstable solutions are called saddles and are shown by dotted lines in Figs. 1–23.

Figures 1–6 show the dependence of the amplitude ρ on the detuning parameter σ on variation of the parameters τ, u and v in the case of primary resonance for the parameters $\mu = 0.5$, $\alpha = 0.4$, $\beta = 1$,

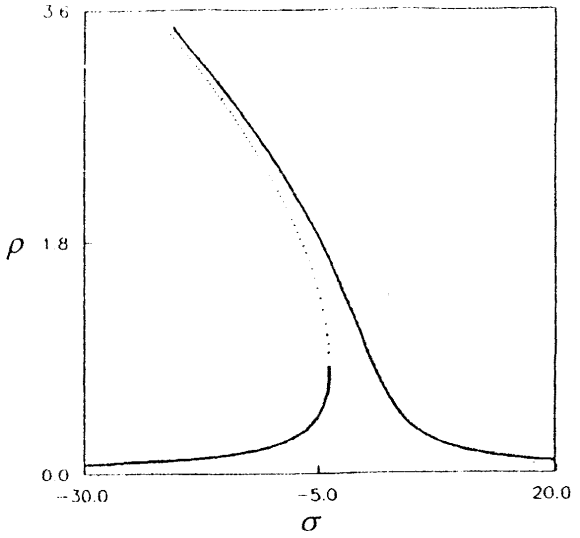

Fig. 1. Frequency-response curve for primary resonances.

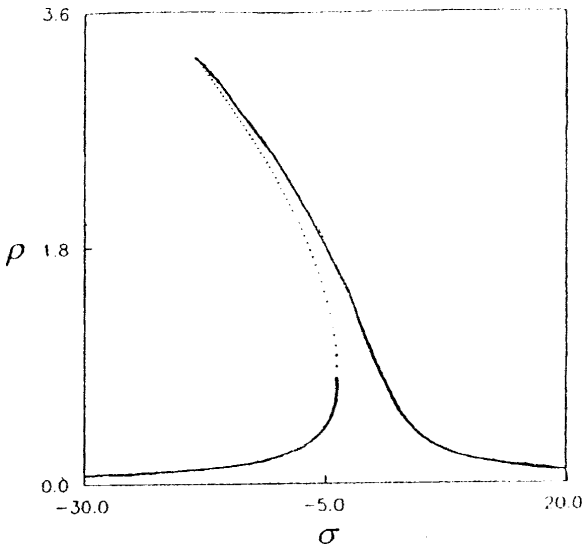

Fig. 2. Frequency-response curve for increasing time delay τ, when $\tau = 1$.

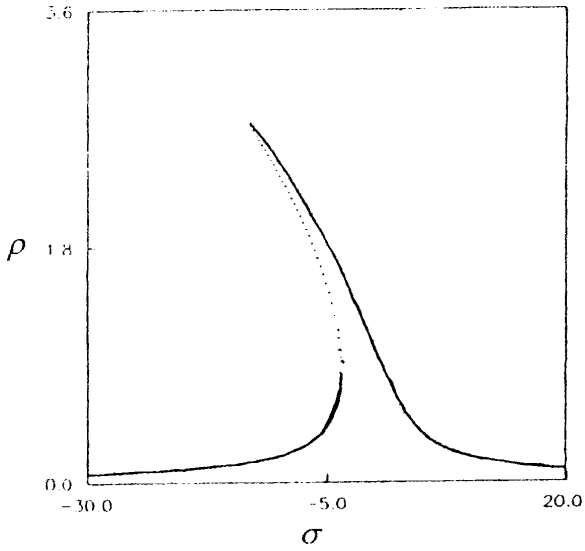

Fig. 3. Frequency-response curve for increasing time delay τ, when $\tau = 2$.

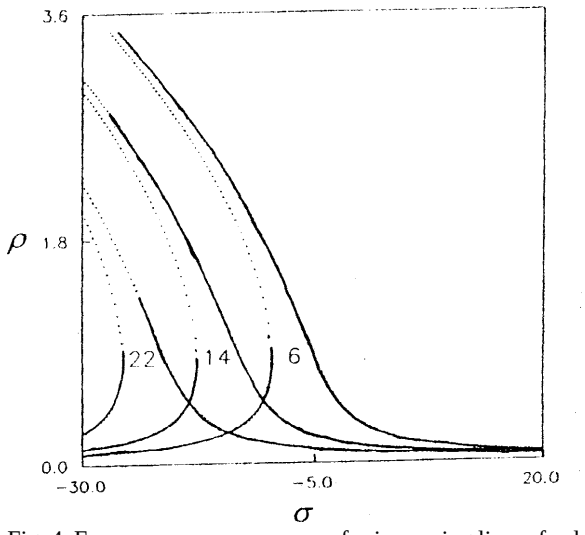

Fig. 4. Frequency-response curves for increasing linear feedback gain u.

$\gamma = 6$, $u = 0.2$, $v = 0.1$, $\tau = 0$ and $H = 4$. In Fig. 1 we note that the amplitude consists of two branches which are bent to the left. The right branch is stable and the left branch is partly stable and partly unstable. As σ increases in the region -30 to -6, the left branch loses stability via a saddle node bifurcation, and there exist jump phenomena. When increasing the time delay τ, the two branches connect and give one branch. The maximum value decreases and there exists a jump phenomenon (Fig. 2). When the time delay τ increases to 2, the maximum of the response amplitude decreases and there exists a jump phenomenon (Fig. 3). When the linear feedback u increases, we observe that the response amplitude shifts to the left and the multi-valued stability zones decrease and increase, respectively. The right branch is stable and there exists a saddle node bifurcation on the left branch. As u takes the values 14 and 22, the two branches shift to the left and the right branch has stable and unstable solutions. As σ increases or decreases, the left and right

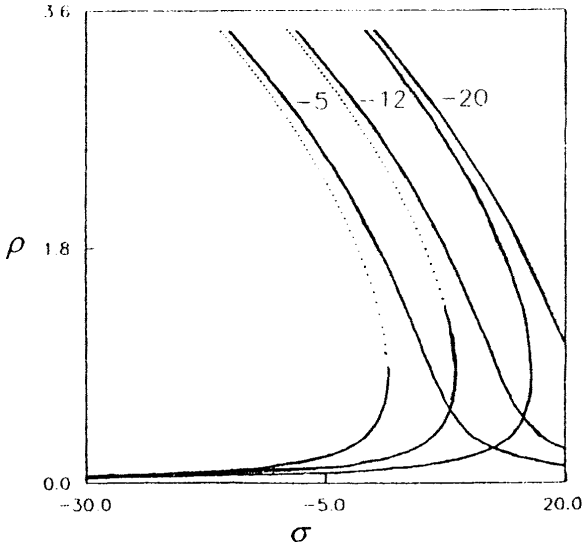

Fig. 5. Frequency-response curves for negative decreasing linear feedback gain u.

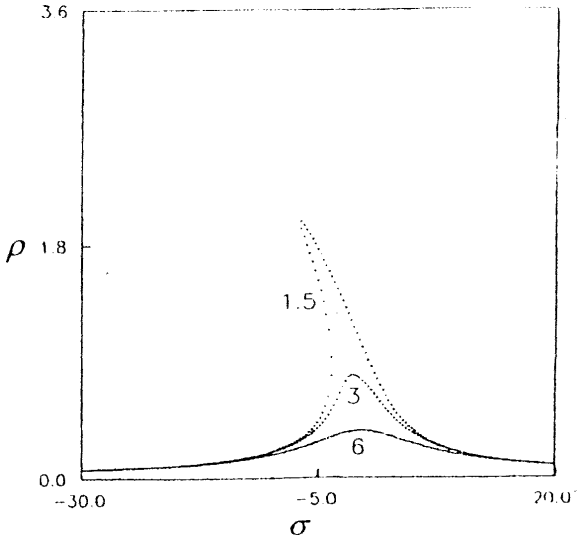

Fig. 6. Frequency-response curves for increasing linear feedback gain v.

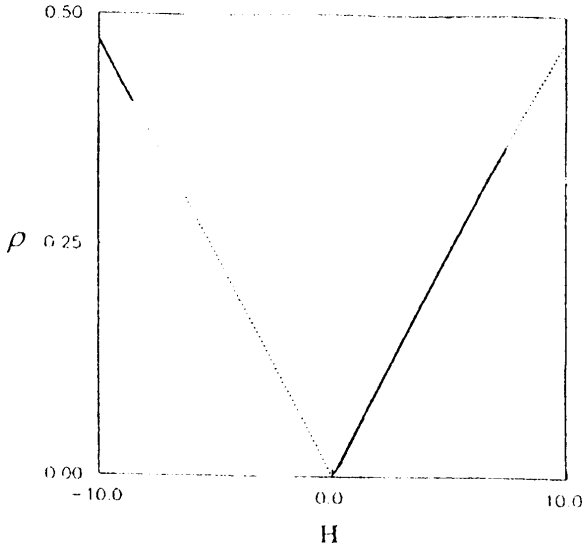

Fig. 7. External excitation H response curves for primary resonances.

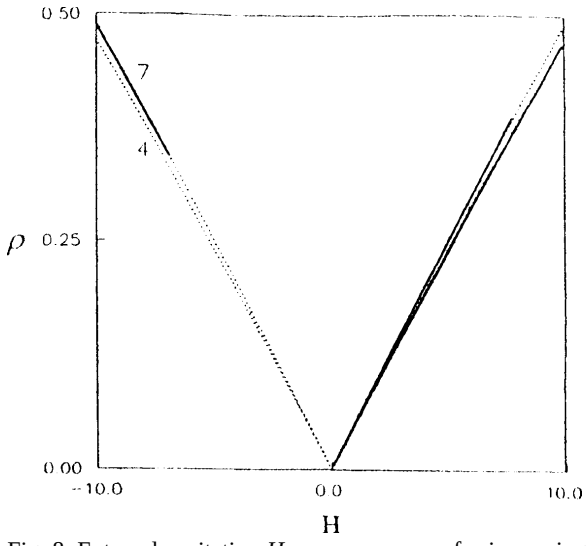

Fig. 8. External excitation H response curves for increasing time delay τ.

branches lose stability via saddle node bifurcations. Figure 4 shows that there exist jump phenomena. On decreasing the linear negative feedback u, the response amplitude shifts to the right. When in Fig. 5 u takes the values -5 and -12, the left branch, corresponding to each value, has a saddle node bifurcation, and when $u = -20$, the saddle node bifurcation disappears and all solutions become stable. When in Fig. 6 the linear feedback v increases, the bent of the response amplitude disappears with unstable decreased magnitudes. Note that this variation corresponds to a decreasing v with negative values (-0.5, -2 and -6).

Figures 7–12 show the variation of the response amplitude ρ with the coefficient of external excitation H for the parameters: $\mu = 0.5$, $\alpha = 0.4$, $\beta = 1$, $\gamma = 6$, $u = 0.2$, $v = 0.1$, $\tau = 0$ and $\sigma = 10$. In Fig. 7 we note that the response amplitude is single-valued and symmetric about $H = 0$. It has stable and unstable solutions. There exist three saddle node bifurcations. Figure 8 shows that for a increasing time delay τ the

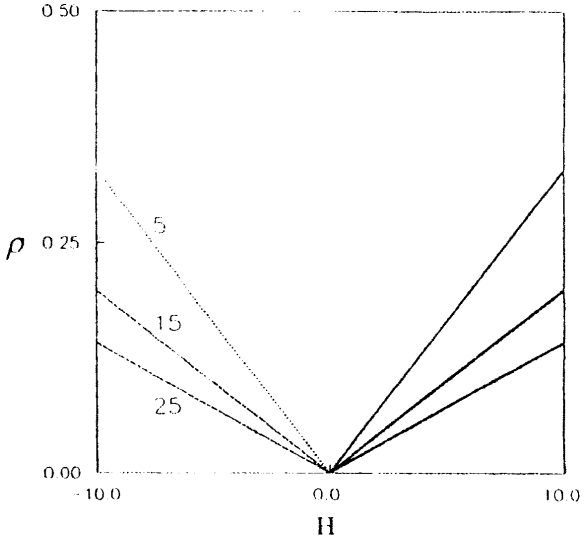

Fig. 9. External excitation H response curves for increasing linear feedback gain u.

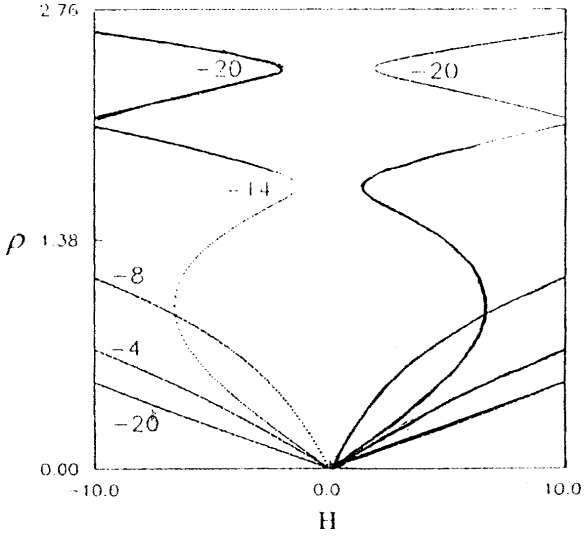

Fig. 10. External excitation H response curves for decreasing linear feedback gain u (negative values).

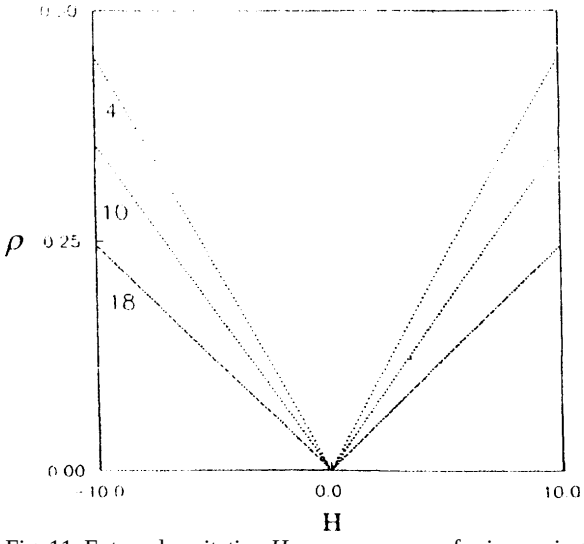

Fig. 11. External excitation H response curves for increasing linear feedback gain v.

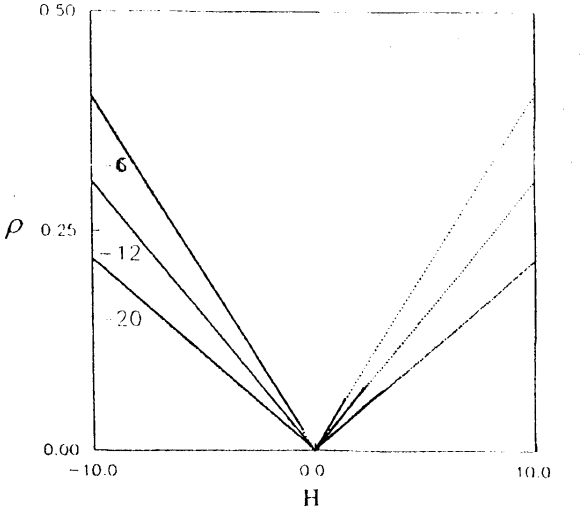

Fig. 12. External excitation H response curves for decreasing linear feedback gain v (negative values).

symmetric single-valued curve decreases somewhat. The left branch has unstable solutions, and there exist two saddle node bifurcations. When the time delay τ increases up to 7, the symmetric single-valued curve increases somewhat. The zone of stability on the left branch increases, but the right branch has stable solutions and there exist two saddle node bifurcations. In Fig. 9 we note that, when the linear feedback u increases, the left branch has unstable solutions and the right branch stable ones. Figure 10 shows the decreasing linear feedback u with negative values. When u takes the values -4 and -8, the symmetric single-valued curve has increased values such that the left branch has unstable solutions and the right branch has stable ones. As u decreases up to -14, the response amplitude becomes a symmetric multi-valued curve. The region of stability is increased and there exist three saddle node bifurcations. For $u = -20$ we note that the response amplitude has four branches, two single-valued branches and two semi-ovals. The two single-valued branches are symmetric about $H = 0$ and de-

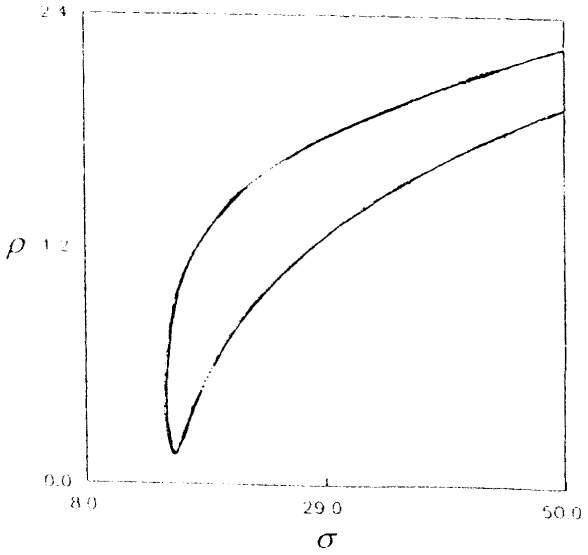

Fig. 13. Frequency-response curve for subharmonic resonances.

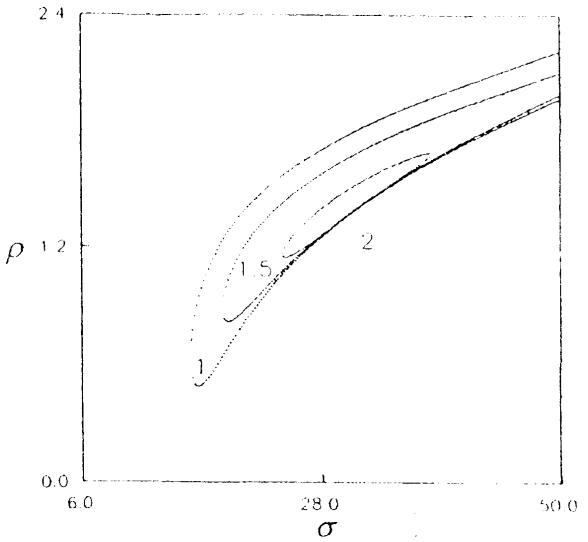

Fig. 14. Frequency-response curves for increasing time delay τ.

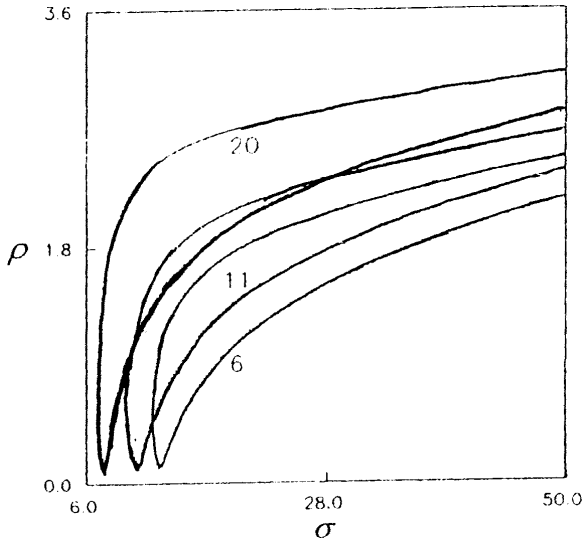

Fig. 15. Frequency-response curves for increasing linear feedback gain *u*.

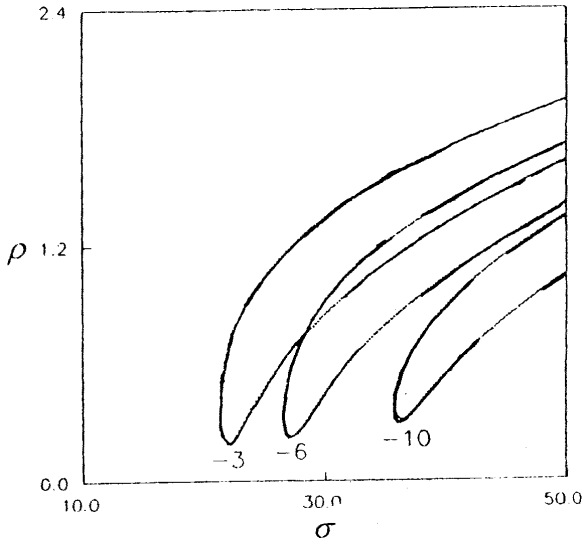

Fig. 16. Frequency-response curves for decreasing linear feedback gain *u* (negative values).

crease such that the left branch has unstable solutions while the right branch has stable solutions. The two semi-ovals have increased magnitudes such that the left branch has stable solutions and the right branch has unstable solutions. When in Fig. 11 the linear feedback v increases, we get similar variations as in Fig. 9, and all solutions are unstable. When v decreases with negative values, we get a similar variation as in Fig. 9, such that the left branch has stable solutions, and as H increases in the region $0-10$, we observe in Fig. 12 that the response amplitude loses stability via a saddle node bifurcation for each value.

Figures 13 – 18 show the frequency-response curves for variation of the parameters τ, u and v in case of subharmonic resonance with the parameters $\mu = 0.5$, $\alpha = 10$, $\beta = 3$, $\gamma = 0.5$, $u = 2$, $v = 1$, $\tau = 0$ and $H = 10$. These figures represent the variation of the response amplitude ρ with the detuning parameter σ. In Fig. 13 we note that the amplitude is multi-valued. It bents to the right and has harding spring vibrations. The re-

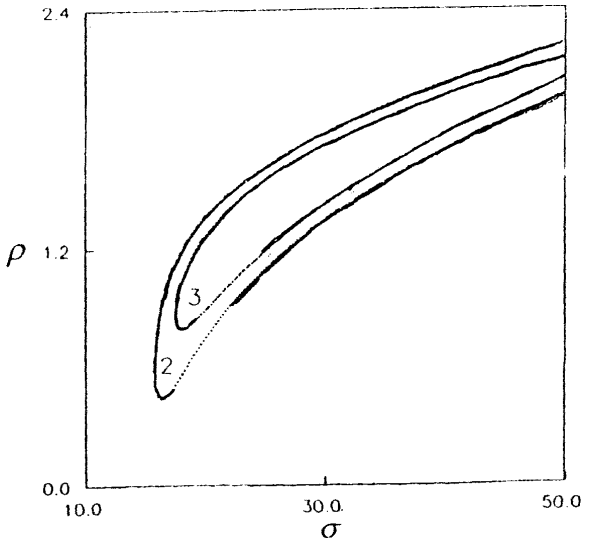

Fig. 17. Frequency-response curves for increasing linear feedback gain v.

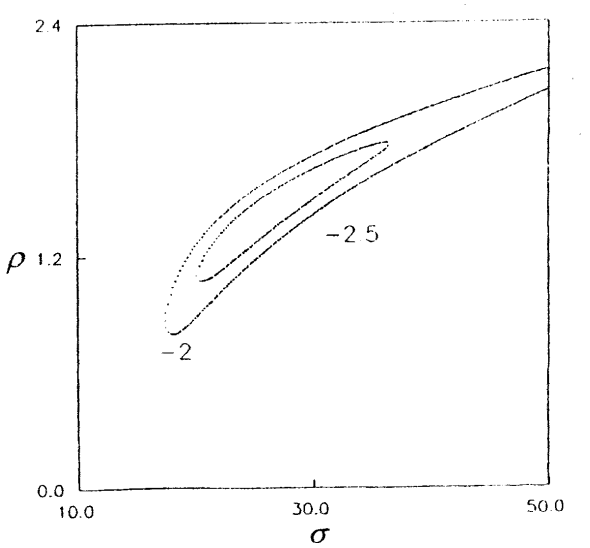

Fig. 18. Frequency-response curves for decreasing linear feedback gain v (negative values).

gions of stability are discontinuous and there exist saddle node bifurcations. If in Fig. 14 the time delay τ is 1 to 1.5, the multi-valued curve contracts and the solution becomes unstable. When in Fig. 15 the linear feedback u is increased (i.e u takes the values 6, 11, and 20), the curves shift to the left and become bigger. As in Fig. 16 u takes the values -3, -6 and -10, we note that the curves shift to the right and move up. As in Fig. 17 the linear feedback v increases, the multi-valued curves become narrower. There exist two saddle

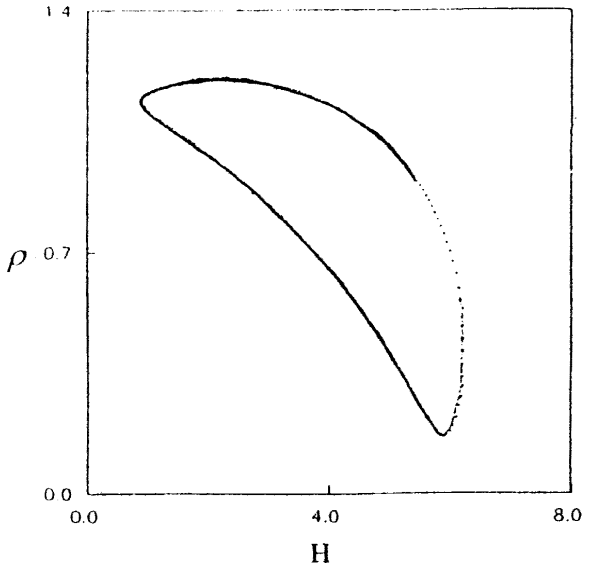

Fig. 19. External excitation-response curve for subharmonic resonances.

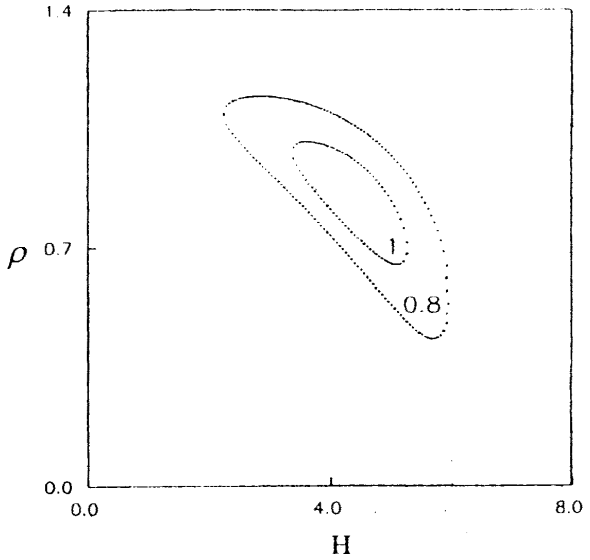

Fig. 20. External excitation-response curves for increasing times delay τ.

node bifurcations. When in Fig. 18 v decreases, we get the same variation as in Fig. 14, and all solutions are unstable.

Figures 19–23 show the external excitation-response curves for the parameters τ, u and v in the case of subharmonic resonance with the parameters $\mu = 0.1$, $\alpha = 10$, $\beta = 3$, $\gamma = 0.5$, $u = 2$, $v = 1$, $\tau = 0$ and $\sigma = 10$. These figures represent the variation of the response amplitude ρ with the coefficient

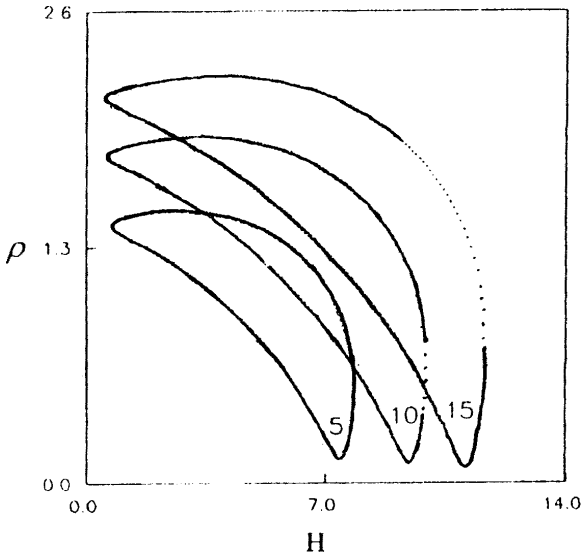

Fig. 21. External excitation-response curves for increasing linear feedback gain *u*.

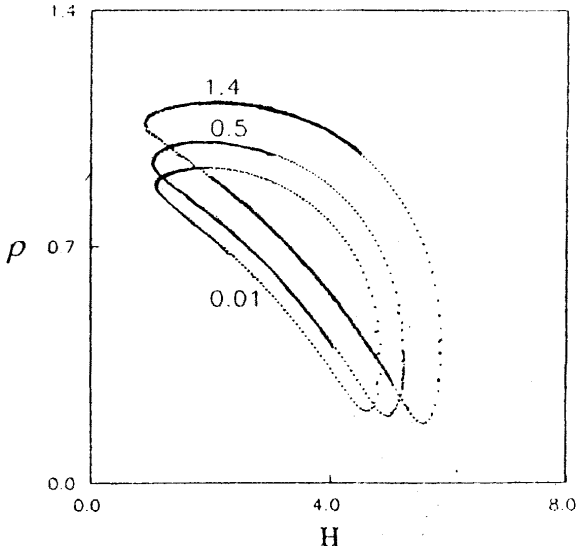

Fig. 22. External excitation-response curves for decreasing linear feedback gain *u* (negative values).

of external excitation H. In Fig. 19 we observe that the response amplitude forms a closed curve which reduces to an oval, and there exist stable and unstable solutions. As H increases, we note that the response amplitude loses stability via saddle node bifurcations. Figure 20 shows that increasing time delay τ the oval contracts and has unstable decreasing magnitudes. Figure 21 shows that as the linear feedback u increases, the closed curves shift to the right with increased stable

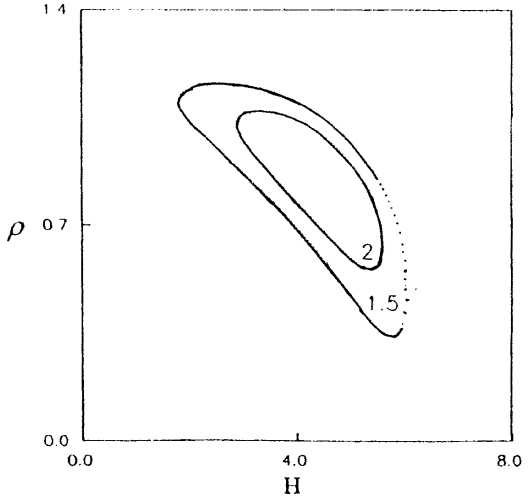

Fig. 23. External excitation-response curves for increasing linear feedback gain *v*.

magnitudes. Each closed curve has two saddle node bifurcations. According to Fig. 22, for decreasing linear feedback u the closed curves shift to the left. The zones of stability are decreased and each has two saddle node bifurcations. According to Fig. 23, as the linear feedback v increases, the closed curves contract such that there exist two saddle node bifurcations for $v = 1.5$ and all solutions are stable for $v = 2$.

5. Concluding Remarks

The time delay in feedback control results in an infinite dimension for the controlled nonlinear system and increases dramatically the complexity of the numerical analysis for the system dynamics. The method of multiple scales proves to be a powerful tool to gain insight into the fundamental and principal resonance of systems having one-degree-of-freedom with weak nonlinearities and weak delay feedback. We have derived two slow-flow equations governing the amplitude and phase of approximate long-time response of the oscillator. Determination of various types of steady-state motion is then reduced to the solution of sets of algebraic equations. The condition for the existence of a stable solution is determined. The solution of the frequency-response equation for the two cases allows for the following conclusions:

- From the frequency-response curves of primary resonance we note that the response amplitude bending to the left, which leads to softening vibration, except for the variation of large values of v. The multi-

valuedness disappears when v takes the values 3 and 6. The solution is stable when $u = -20$. The response amplitude loses stability for large values of v. The response amplitude shifts to the left and to the right for increasing and decreasing u, respectively.

• From the parametric excitation-response curves of primary resonance we note that the excitation-response curves are symmetric about $H = 0$. The response amplitude loses stability for increasing u. The response amplitude shifts down with decreasing magnitudes by increasing v, respectively, and also for decreasing v with negative values. The response amplitude is multi-valued when $u = -14$. The response amplitude is four branches (two single-valued and two semi-oval ones), when $u = -20$.

• From the frequency-response curves of subharmonic resonances we note a response amplitude bending to the right, which leads to hardening the vibration. The response amplitude loses stability for increasing and decreasing u and v, respectively. The zone of definition is increased and decreased for increasing and decreasing u, respectively. The response amplitude becomes oval, when $\tau = 2$ and $v = -2.5$.

• From the parametric excitation-response curves of subharmonic resonance we note a response amplitude bending to the left which leads to softening vibration. The response amplitude loses stability for increasing and decreasing time delay τ. All solutions are stable, when $u = 5$ and $v = 2$. The response amplitude shifts to the left and moves with increased magnitude for increasing u, respectively. The region of definition is increased and decreased for increasing and decreasing u and v, respectively.

[1] R. H. Plaut and J. C. Hsieh, J. Sound Vib. **117**, 497 (1987).
[2] L. Palkovics and P. J. Venhovens, Vehicle Syst. Dyn. **21**, 269 (1992).
[3] J. Belair and S. A. Cambell, SIAM J. Appl. Math. **54**, 1402 (1994).
[4] O. Diekmann, S. A. Van Gils, S. M. Verduyn Lunel, and H. O. Walther, Delay Equations, Functional, Complex, and Nonlinear Analysis, Springer-Verlag, New York 1995.
[5] G. Stepan and G. Haller, Nonlinear Dyn. **8**, 513 (1995).
[6] J. L. Moiola, H. G. Chiacchiarini, and A. C. Desages, Int. J. Bifurcation Chaos **64**, 661 (1996).
[7] J. J. Thomsen, J. Sound Vib. **197**, 403 (1996).
[8] H. Yabuno, Nonlinear Dyn. **12**, 236 (1997).
[9] H. Hu, E. H. Dowell, and L. N. Virgin, Nonlinear Dyn. **15**, 311 (1998).
[10] H. Hy and W. Zh, Prog. Nat. Sci. **10**, 801 (2000).
[11] A. Maccari, Nonlinear Dyn. **26**, 105 (2001).
[12] T. Faria, J. Math. Anal. Appl. **63**, 254 (2001).
[13] X. Liao and G. Chen, Int. J. Bifurcat. Chaos **11**, 2105 (2001).
[14] X. Meng and J. Wei, Chaos, Solitons and Fractals **21**, 729 (2004).
[15] S. Yuan and M. Han, Chaos, Solitons and Fractals **20**, 995 (2004).
[16] M. S. Fofance and P. B. Ryba, Int. J. Nonlinear Mech. **23**, 79 (2004).
[17] A. Y. T. Leung, J. C. Ji, and G. Chen, Int. J. Bifurcation Chaos **14**, 1423 (2004).
[18] Z. Sun, W. Xu, X. Yang, and T. Fang, Chaos, Solitons and Fractals **27**, 705 (2006).
[19] X. Li, J. C. Ji, C. H. Hansen, and C. Tan, J. Sound Vib. **291**, 644 (2006).
[20] A. F. El-Bassiouny, Shock Vib. **13**, 65 (2006).
[21] A. Kouda and S. Mori, IEEE Trans. Circuits Syst. **28**, 247 (1981).
[22] S. S. Oueni, A. H. Nayfeh, and J. R. Pratt, Nonlinear Dyn. **15**, 259 (1998).
[23] S. S. Oueni, C.-M. Chen, and A. H. Nayfeh, Nonlinear Dyn. **20**, 283 (1999).
[24] A. F. El-Bassiouny, Phys. Scr. **72**, 203 (2005).
[25] A. F. El-Bassiouny, Physica A **366**, 167 (2006).
[26] L. D. Zavodney and A. H. Nayfeh, Int. J. Nonlinear Mech. **24**, 105 (1989).
[27] A. H. Nayfeh and D. T. Mook, Nonlinear Oscillations, Wiley, New York 1979.
[28] A. H. Nayfeh, Perturbation Techniques, Wiley, New York 1981.
[29] A. F. El-Bassiouny, Mech. Res. Commun. **32**, 337 (2004).
[30] A. R. F. Elhefnawy and A. F. El-Bassiouny, Chaos, Solitons and Fractals **23**, 289 (2004).
[31] A. F. El-Bassiouny and M. Eissa, Phys. Scr. **70**, 101 (2004).